15 October 2001

ELSEVIER

Optics Communications 198 (2001) 217–226

OPTICS COMMUNICATIONS

www.elsevier.com/locate/optcom

Two-zone double phase conjugate mirror

M.R. Belić [a], D. Vujić [b,*], O. Sandfuchs [c], F. Kaiser [c]

[a] *Institute of Physics, P.O. Box 57, 11001 Belgrade, Yugoslavia*
[b] *Faculty of Sciences, University of Kragujevac, P.O. Box 60, 34000 Kragujevac, Yugoslavia*
[c] *Institute of Applied Physics, Darmstadt University of Technology, Hochschulstrasse 4a, D-64289 Darmstadt, Germany*

Received 2 February 2001; received in revised form 4 August 2001; accepted 7 August 2001

Abstract

An analysis of photorefractive (PR) oscillators consisting of two facing four-wave mixing regions is carried out. The threshold and operation conditions of different phase conjugate mirrors are discussed with the help of the grating action method. In particular, the threshold and the operation of the two-zone double phase conjugate mirror (DPCM) is compared with other related PR oscillators, the interconnected ring, and different connected DPCM. © 2001 Elsevier Science B.V. All rights reserved.

PACS: 42.65.Hw; 42.65.−k

Keywords: Phase conjugate mirrors; Four-wave mixing; Photorefractive oscillators; Grating action method

1. Introduction

In an interesting paper [1] Wolffer and Gravey introduced a novel double phase conjugate mirror (DPCM) geometry which, in their words, leads to a "dramatic improvement of phase conjugation quality". It is a clever arrangement, depicted in Fig. 1(a), with two photorefractive (PR) crystals and an aberrating lens in between. The authors experimentally display how this device, termed the two-zone (2Z) DPCM, overcomes main difficulties associated with the double phase conjugation process, namely the conical diffraction and instabilities. Along the way they make a puzzling statement, that their device "will have the same threshold and efficiency as the mutually pumped phase conjugator (MPPC) of Ref. [2] in the one-dimensional model, or as a DPCM with twice the length of an individual crystal". Our paper, among other things, is devoted to clarifying this statement. We find the situation a bit more complex.

The puzzle is created after one inspects the conjugator of Zozulya and Mamaev [2]. It is an interconnected ring (ICR) mirror, displayed in Fig. 1(b). Under normal conditions, rings and DPCMs have different threshold and operation points [3–5]. The source of the statement is revealed at the same place. The authors further state that "the 2Z-DPCM belongs to a family of MPPC mirrors, whose similarities have been pointed out by Cronin-Golomb [6]". Indeed, in Ref. [6] one finds the statement that "the ICR mirror with interaction length l and perfect feedback is equivalent to a DPCM of length $2l$ with equal-intensity

* Corresponding author.
E-mail address: dvujic@knez.uis.kg.ac.yu (D. Vujić).

PII: S0030-4018(01)01500-0

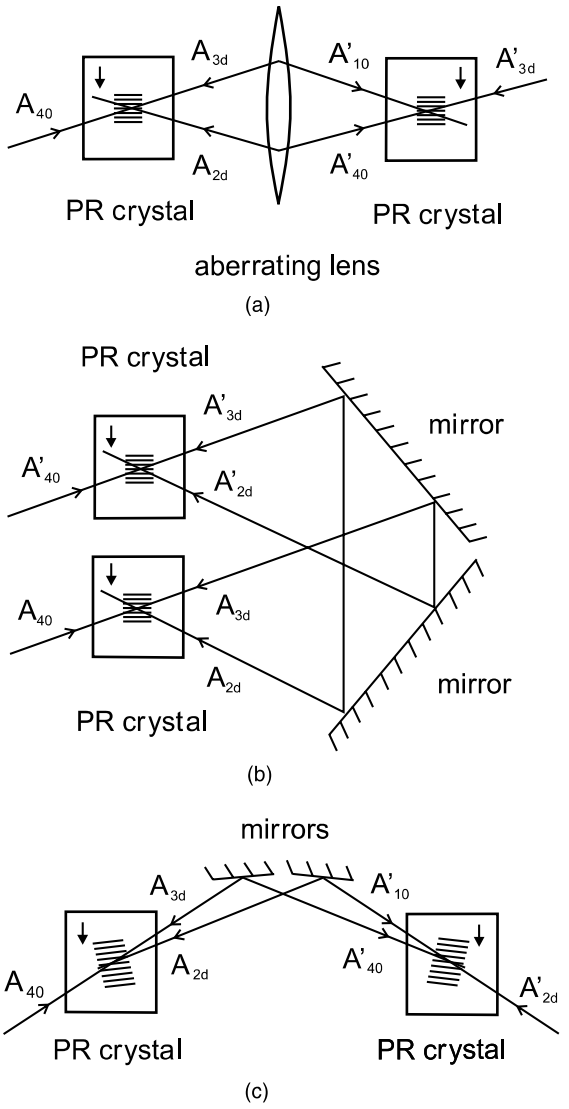

Fig. 1. Three basic conjugator geometries with two crystals, analyzed in the text. (a) 2Z-DPCM. (b) ICR mirror. (c) Connected DPCM with two IR. Ruled regions within each of the crystals denote induced gratings, short arrows indicate the directions of *c*-axes.

input beams''. Cronin-Golomb establishes the equivalence by an ingenious sequence of topological manipulations. However, there is more to the operation of these devices than topological equivalence. It is our intention to put these statements on a more firm mathematical foundation, and to provide for a more rigorous comparison of these devices. More generally, our goal is to discuss and compare different PR oscillators that consist of two facing four-wave mixing (4WM) interacting regions connected in different ways, from a unifying point of view.

To this end, we cast the results on all geometries in the same language of the grating action theory [4,7,8]. It applies to the steady-state plane-wave representation of the 4WM process, which is at the core of operation of any PR oscillator. In this manner we will be able to compare different geometries on an equal footing. Six geometries will be compared, presented in Figs. 1 and 2. They include 2Z-DPCM, the ICR, and different geometries of the two facing DPCMs. We show that under certain circumstances the thresholds of some geometries can coincide, but that, in general, this is

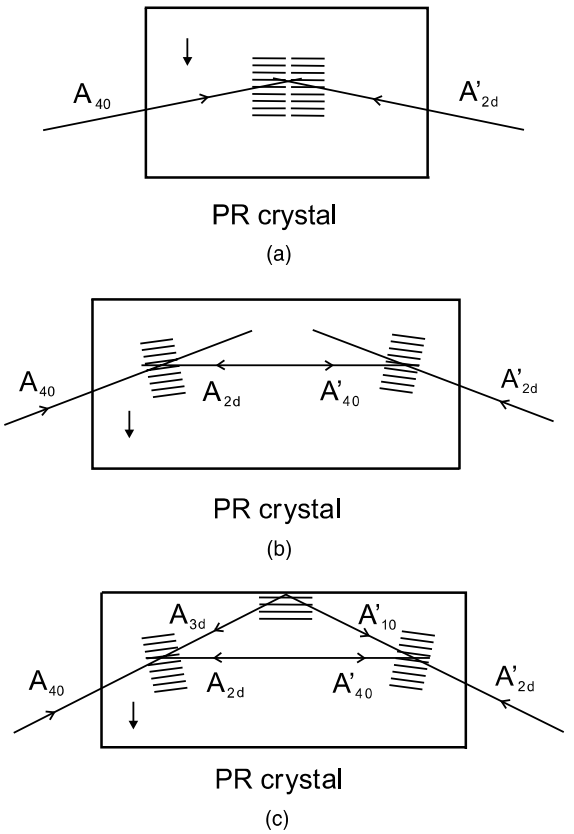

Fig. 2. Three DPCM with two IRs within one crystal. (a) DPCM of length 2*l*. (b) Lossy DPCM. (c) Conserved DPCM. The upper optical path can be closed either by TIR or by another IR.

not the case. While the geometries in Fig. 1, 2Z-DPCM, ICR, and the connected DPCM are closely related, the geometries of Fig. 2, the DPCM of length $2l$, the lossy DPCM, and the conserved DPCM are unrelated to them. We further show that the operation of the devices in Figs. 1 and 2 is quite different from each other.

A number of geometries of two facing DPCMs is used, as shown in Figs. 1 and 2. This is because the two DPCMs can be connected in more than one way, with different results. The connected DPCM of Fig. 1(c), by construction, is related to ICR, as well as 2Z-DPCM. The purpose of this geometry is to show that there exists a straightforward connection of two DPCMs which is closer to 2Z-DPCM than the supposed DPCM of length $2l$. The difference between the three geometries in Fig. 2 is more pronounced. Fig. 2(a) is the simple DPCM of length $2l$. Its behavior is well known [3,9], however it is needed here for comparison with 2Z-DPCM, as it is specifically mentioned in Refs. [1,6]. The difference between the devices in Fig. 2(b) and (c) is that in the first one the strayed beams from IRs are lost, whereas in the second one they are collected by the other IR. Hence, a part of energy is lost in the first geometry, and this shows on the operation and the threshold of the device. We call the first geometry the lossy DPCM, and the second one the conserved DPCM [10]. It should be mentioned that the strayed beams in the conserved DPCM can be collected in different ways, for example by the total internal reflection (TIR) off the upper crystal face or by the formation of the third IR. The physics of the device with three IRs is somewhat different from the physics of device with two IRs, however the mathematics is the same.

Section 2 of the paper contains an outline of the grating action method, Section 3 presents results of the application to the geometries at hand, Section 4 provides an analysis of the results, and Section 5 brings conclusions.

2. Grating action method

The basic quantity of the method, in terms of which the output beams are represented as functions of the input beams, is the grating action [4,7,8]

$$u = \frac{1}{d}\int_0^d \frac{\Gamma|Q|}{I}\,\mathrm{d}z, \tag{1}$$

where d is the thickness of IR, Γ is the coupling strength of the 4WM process (coupling constant times the thickness of IR), $Q = A_1\overline{A}_4 + \overline{A}_2A_3$ is the grating amplitude of the four beams, and $I = \sum_{j=1}^{4}|A_j|^2$ is the total intensity. Only transmission gratings (TG) are considered, even though it presents no difficulty to extend the analysis to reflection gratings (RG) [11]. Steady-state, plane-wave, and degenerate situation is assumed, and absorption, as well as nonlinearities arising at the high fringe modulation are neglected. The grating action is found from the expression

$$(A_{10}\overline{A}_{40} + \overline{A}_{2d}A_{3d} + \text{c.c.})\cot u + I_{10} - I_{2d} + I_{3d} - I_{40} = aI\coth\left(\frac{a\Gamma}{2}\right), \tag{2}$$

where the subscripts 0 and d denote the entrance/exit faces of an IR, and the overbar stands for complex conjugation. The constant a is found from the conserved quantity

$$a^2I^2 = (I_1 + I_2 - I_3 - I_4)^2 + 4|Q|^2. \tag{3}$$

The expressions (2) and (3) should be applied to each IR, or to each crystal comprising the given PR conjugator, keeping the track of all beams. In this manner one obtains a system of algebraic equations for u's and a's. Real devices or PC mirrors are formed by connecting output beams of one or more IR with the input beams, using external mirrors or TIRs within the crystal. We report the expressions for all geometries, then comment on the similarities and differences between them. In all the cases there are two IR, one of which is denoted by a prime.

3. Results

3.1. Two-zone double phase conjugate mirror

In the case of 2Z-DPCM one obtains

$$\cos(u - u') = \frac{1 + |tq|^2}{2|tq|}\sqrt{1 - a'^2}, \tag{4a}$$

$$1-\sigma' = |tq|\frac{\sin u}{\sin u'}\sqrt{1-a'^2} \tag{4b}$$

for the primed region, and

$$\cos(u-u') = \frac{|t|^2+|q|^2}{2|tq|}\sqrt{1-a^2}, \tag{4c}$$

$$1+\sigma = \frac{|t|}{|q|}\frac{\sin u'}{\sin u}\sqrt{1-a^2} \tag{4d}$$

for the unprimed region. The symbol σ stands for $a\coth(a\Gamma/2)$, $|q|^2 = |A_{40}|^2/|A'_{3d}|^2$ is the ratio of input intensities, and $|t|^2$ the transmissivity of optical paths through the lens. The device transmissivity and reflectivity are given by

$$T = \frac{|A'_{1d}|^2}{|A_{40}|^2} = \frac{|A_{20}|^2}{|A'_{3d}|^2} = |t|^2\cos^2(u-u'), \tag{5a}$$

$$R = \frac{|A_{30}|^2}{|A_{40}|^2} = \frac{1}{|q|^4}\frac{|A'_{4d}|^2}{|A'_{3d}|^2} = \frac{|t|^2}{|q|^2}\sin^2(u-u'). \tag{5b}$$

3.2. Interconnected ring

The corresponding expressions for ICR are of the form

$$\cos(u+u') = \frac{1+|tq|^2}{2|tq|}\sqrt{1-a'^2}, \tag{6a}$$

$$1+\sigma' = -|tq|\frac{\sin u}{\sin u'}\sqrt{1-a'^2} \tag{6b}$$

for the primed region, and

$$\cos(u+u') = \frac{|t|^2+|q|^2}{2|tq|}\sqrt{1-a^2}, \tag{6c}$$

$$1+\sigma = -\frac{|t|}{|q|}\frac{\sin u'}{\sin u}\sqrt{1-a^2} \tag{6d}$$

for the unprimed region. $|q|^2 = |A_{40}|^2/|A'_{40}|^2$ is again the ratio of input intensities, and $|t|^2$ the transmissivity of loops involving external mirrors (equal to the product of mirror reflectivities). The device transmissivity and reflectivity are

$$T = \frac{|A'_{20}|^2}{|A_{40}|^2} = \frac{|A_{20}|^2}{|A'_{40}|^2} = |t|^2\cos^2(u+u'), \tag{7a}$$

$$R = \frac{|A_{30}|^2}{|A_{40}|^2} = \frac{1}{|q|^4}\frac{|A'_{30}|^2}{|A'_{40}|^2} = \frac{|t|^2}{|q|^2}\sin^2(u+u'). \tag{7b}$$

3.3. Connected double phase conjugate mirror

The expressions for the connected DPCM are the same as the expressions for ICR, even though the coupling of the beams in the two 4WM regions is achieved differently. The definitions of the transmissivity and the reflectivity must reflect this different coupling of the beams:

$$T = \frac{|A'_{4d}|^2}{|A_{40}|^2} = \frac{|A_{20}|^2}{|A'_{2d}|^2}, \tag{8a}$$

$$R = \frac{|A_{30}|^2}{|A_{40}|^2} = \frac{1}{|q|^4}\frac{|A'_{1d}|^2}{|A'_{2d}|^2}. \tag{8b}$$

3.4. Double phase conjugate mirror with double the interaction length

The expressions for the DPCM of length $2d$ are the familiar expressions [8,9,11] for the simple DPCM:

$$\cos(2u) = \frac{1+|q|^2}{2|q|}\sqrt{1-a^2}, \tag{9a}$$

$$1+\sigma = 0, \tag{9b}$$

except that they involve $2u$ in Eq. (9a) and 2Γ in the expression for σ. The ratio of input intensities is $|q|^2 = |A_{40}|^2/|A'_{2d}|^2$, and the device transmissivity and reflectivity are

$$T = \frac{|A'_{1d}|^2}{|A_{40}|^2} = \cos^2 2u, \tag{10a}$$

$$R = \frac{|A_{30}|^2}{|A_{40}|^2} = |q|^2\sin^2 2u. \tag{10b}$$

For a lack of better word, we call this device the double DPCM.

3.5. Lossy double phase conjugate mirror

The lossy DPCM represents a slight complication over the simple DPCM, however the equations look quite different:

$$\cos u' = -\frac{1+|q|^2\sin^2 u}{2|q|\sin u}\sqrt{1-a'^2}, \tag{11a}$$

$$1+\sigma' = 0 \tag{11b}$$

for the primed region, and

$$\cos u = -\frac{|q|^2+\sin^2 u'}{2|q|\sin u'}\sqrt{1-a^2}, \tag{11c}$$

$$1+\sigma = 0 \tag{11d}$$

for the unprimed region. The transmissivity and the reflectivity are

$$T = \frac{|A'_{1d}|^2}{|A_{40}|^2} = \frac{|A_{30}|^2}{|A'_{2d}|^2} = \sin^2 u' \sin^2 u, \tag{12a}$$

$$R = \frac{|A_{30}|^2}{|A_{40}|^2} = \frac{1}{|q|^4}\frac{|A'_{1d}|^2}{|A'_{2d}|^2} = \frac{\sin^2 u' \sin^2 u}{|q|^2}. \tag{12b}$$

3.6. Conserved double phase conjugate mirror

The conserved DPCM is considerably more complicated, owing to the singular nature of the new optical path. It is realized in two geometries, one with TIR and the other with three IRs. The physics of the two realizations is different, in that the geometry with TIR includes cross-talk between the reflected and the phase conjugated beam, whereas the geometry with three IRs is without cross-talk. In addition, the threshold and operation conditions of the device with three IRs is different from the device with two IRs. These differences have been discussed elsewhere [12]. Here we will stay within the realm of two IR devices, and use the reflectivity of the third IR only as a parameter in the operation. Then the mathematics of the two devices is the same.

For ease of comparison with other devices, it is also assumed that the beams interfere constructively in both IRs. The grating action method provides for the following relations:

$$|\cos u' \sin u - t\cos u \sin u'| = \frac{1+|qt|^2\cos^2 u+|q|^2\sin^2 u}{2|q|}\sqrt{1-a'^2}, \tag{13a}$$

$$1+\sigma' = \frac{|q|\cos u[|t|^2\cos u - \Re(t)\cot u' \sin u]}{|\cos u' \sin u - t\cos u \sin u'|}\sqrt{1-a'^2} \tag{13b}$$

for the primed region, and

$$|\cos u \sin u' - t\cos u' \sin u| = \frac{|q|^2+|t|^2\cos^2 u'+\sin^2 u'}{2|q|}\sqrt{1-a^2}, \tag{13c}$$

$$1+\sigma = \frac{\cos u'[|t|^2\cos u' - \Re(t)\cot u \sin u']}{|q||\cos u \sin u' - t\cos u' \sin u|}\sqrt{1-a^2} \tag{13d}$$

for the unprimed region. Here $\Re$ stands for the real part and $|q|^2 = |A_{40}|^2/|A'_{2d}|^2$. The parameter t has different meanings in the two geometries: it is the transmissivity of the path involving TIR, or it is the reflectivity of the third IR, $t = -\sin u''$. The transmissivity and the reflectivity of the whole device are given by

$$T = \frac{|A'_{1d}|^2}{|A_{40}|^2} = \frac{|A_{30}|^2}{|A'_{2d}|^2} = |t\cos u\cos u' + \sin u \sin u'|^2, \tag{14a}$$

$$R = \frac{|A_{30}|^2}{|A_{40}|^2} = \frac{1}{|q|^4}\frac{|A'_{1d}|^2}{|A'_{2d}|^2} = \frac{|t\cos u\cos u' + \sin u \sin u'|^2}{|q|^2}. \tag{14b}$$

Strictly speaking, in the case of the conserved DPCM with three IRs, one should add the equations for the third region,

$$\cos u'' = \frac{|q|^2\cos^2 u+\cos^2 u'}{2|q|\cos u\cos u'}\sqrt{1-a''^2}, \tag{15a}$$

$$1+\sigma'' = 0, \tag{15b}$$

and consider the system of six equations. Such a system has been considered in Ref. [12] and will not be discussed here. In the further analysis we assume that t is a given parameter.

The conserved DPCM is the most general and the most complicated of all DPCMs with two IRs.

It is tempting to simplify the expressions by taking $t = 1$, however, as it will be seen in the moment, the solutions do not exist then. We proceed to analyze these results.

4. Analysis

The standard analysis of each of the devices is carried out along the following lines. To find steady-state solutions, one solves the four equations for u, u', a, a', for the given values of the parameters Γ, Γ', q, t. To find threshold, one determines the universal relation between a, a', Γ, Γ', and calculates the minimum values of a, a'. The universal relation is obtained by eliminating (when possible) u, u' from the system of equations, leaving a, a' as functions of Γ, Γ'. Substituting the minimum values of a, a', leads to the threshold curve in the plane (Γ, Γ'). This is the procedure for a normal MPPC, which is self-starting, and whose thresholds are located at u, u' equal to 0.

However, there exist conjugators, the lossy DPCM in this case, whose grating actions are not zero at the threshold, and who require a finite seeding to start. The threshold curve in their case is the outline of the projection of the reflectivity surface onto the (Γ, Γ') plane. In other words, normal MPPCs have thresholds where the plane $R = 0$ cuts through the surface $R(\Gamma, \Gamma')$. In the lossy DPCM the surface $R(\Gamma, \Gamma')$ is not cut by the plane (i.e. the equation $R = 0$ has the solution only at $-\infty$). To find the threshold curve, one projects the surface down onto the (Γ, Γ') plane, and takes the outline as the threshold curve. Such a curve does not follow from a universal relation, and is difficult to determine analytically.

To find the operation point of these devices, one evaluates the parameters Γ, Γ' for which the reflectivity reaches a maximum. This generally occurs away from the threshold curve, towards the regions of higher coupling strengths. Naturally, all the analysis is carried out in the region of allowed coupling strengths, bounded by the maximally and minimally attainable (positive and negative) coupling strengths in the given crystal, for the given geometry.

Particular solutions, for given sets of parameters, are of no particular interest. It is more interesting to establish the threshold and operation conditions for the devices. We analyze 2Z-DPCM, the connected DPCM, and ICR concurrently, since they are closely related. In fact, the analysis of the geometry, as well as the equations, reveals that the connected DPCM is equivalent to ICR. Universal relations for 2Z-DPCM and ICR are obtained by combining the equations for σ and σ'. They are of the form

$$(1 - \sigma')(1 + \sigma) = |t|^2 \sqrt{(1 - a'^2)(1 - a^2)} \tag{16}$$

for 2Z-DPCM, and

$$(1 + \sigma')(1 + \sigma) = |t|^2 \sqrt{(1 - a'^2)(1 - a^2)} \tag{17}$$

for ICR. The threshold curves are obtained by substituting the minimum values of a and a'. These are found by considering the limits u, $u' \to 0$ in Eqs. (4a), (4c), (6a) and (6c). Identical expressions are procured for both devices

$$a'_{\text{th}} = \frac{|1 - |tq|^2|}{1 + |tq|^2}, \qquad a_{\text{th}} = \frac{||t|^2 - |q|^2|}{|t|^2 + |q|^2}. \tag{18}$$

A few threshold curves are displayed in Fig. 3. The region of allowed Γ, Γ' lies below the threshold curve. From the graphs it becomes obvious what was suspected all along: 2Z-DPCM is also identical to ICR once the coupling strength Γ' reverses its sign. This is most easily achieved by flipping the

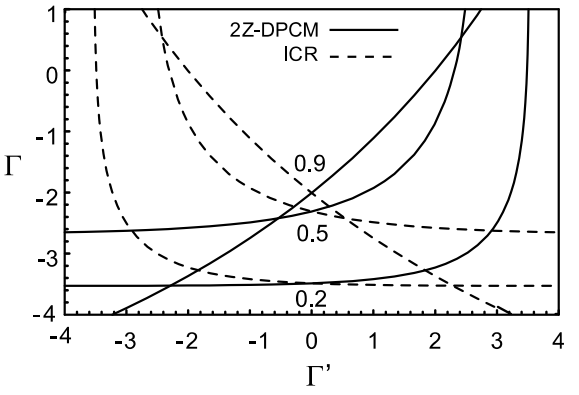

Fig. 3. Threshold curves of 2Z-DPCM (—) and ICR (- - -), for three different values of the transmissivity $|t|$, given in the figure. The ratio of input intensities $|q|^2 = 1$.

second crystal in Fig. 1(a). In other words, 2Z-DPCM and ICR come in two different basic geometries. One is when the c-axes in both crystals are parallel to each other, the other is when the axes are antiparallel. The parallel case of 2Z-DPCM is identical to the antiparallel case of ICR, and conversely. Hence, all of the findings reported in Ref. [11] for the TG interconnected ring apply to the 2Z-DPCM as well. Fig. 4 exemplifies the reflectivity surface as a function of coupling strengths and grating actions. It is noted that 2Z-DPCM provides for an efficient coupling of two 4WM interaction regions, and that it offers other advantages, as described in Ref. [1]. The other DPCM-like couplings provide for a different behavior.

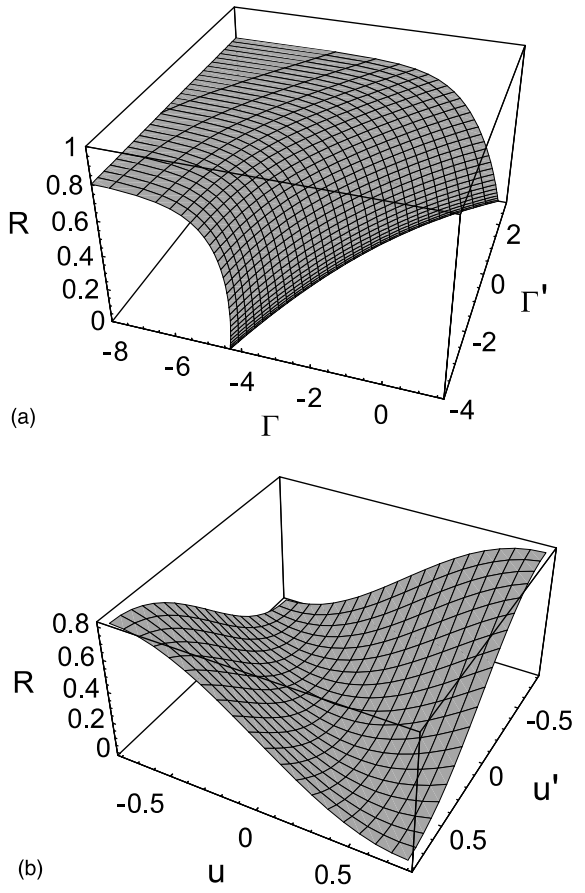

Fig. 4. Reflectivity surface of 2Z-DPCM as a function of (a) coupling strengths Γ, Γ', (b) grating actions u, u'. In both the cases $|q| = 1$, $|t| = 0.9$.

In fact, the three DPCM geometries in Fig. 2 are themselves quite different, although the lossy DPCM is obtained from the double DPCM by taking apart the two IRs, and the conserved DPCM from the lossy DPCM by connecting the upper optical path. The major difference between the three is that the oscillation threshold of the double DPCM and of the conserved device for high enough $|t|$ ($|t| \geqslant 0.23$) is like a second-order phase transition, whereas the threshold of the lossy device is like a first-order phase transition [13]. The threshold curve for the conserved DPCM (and the threshold point for the double DPCM) is located at u, u' equal 0, whereas for the lossy it must be projected down. The threshold condition and the operation of the double DPCM is the same as that of the single DPCM, and is discussed elsewhere [8,9,11]. We touch upon it later, inasmuch as it concerns the comparison with 2Z-DPCM. The threshold curves for the lossy and the conserved devices are depicted in Fig. 5, and the reflectivity surfaces in Fig. 6.

Even though the conserved DPCM for high enough $|t|$ is a normal MPPC, the universal relation between a and a' cannot be determined as an explicit functional dependence for arbitrary t and

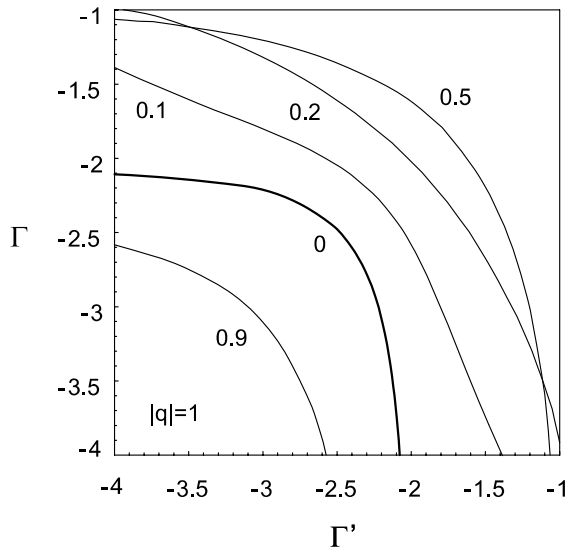

Fig. 5. Threshold curves of DPCM-2IR, for different values of the transmissivity $|t|$, given in the figure. The thick line, for $|t| = 0$, corresponds to the lossy DPCM.

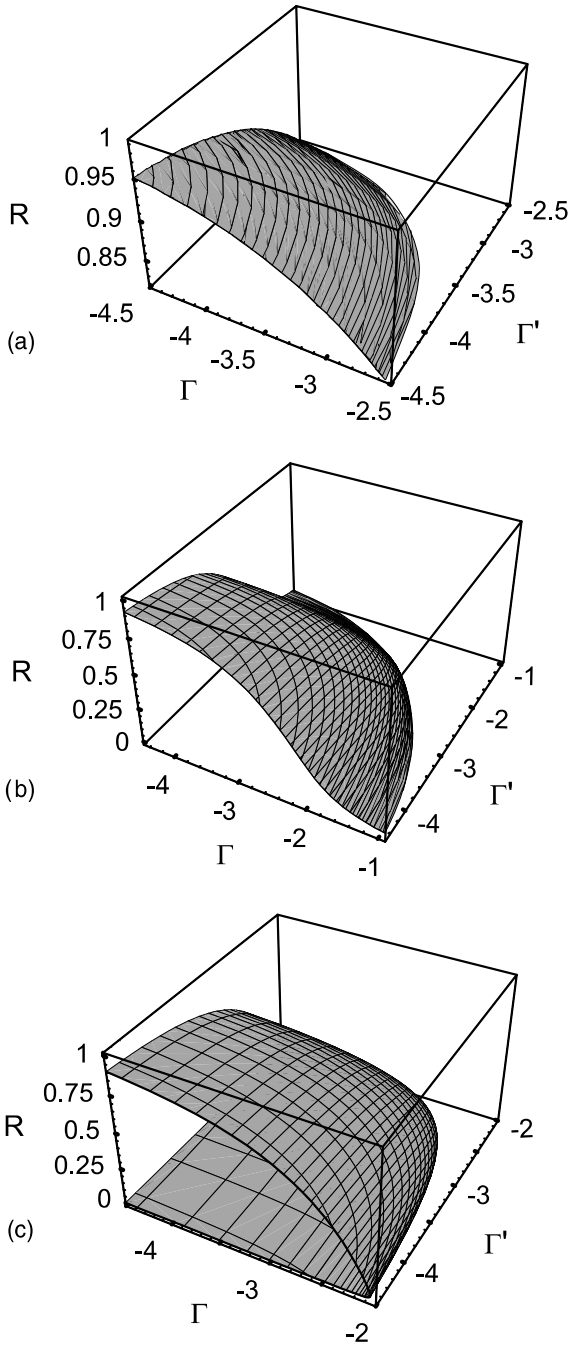

Fig. 6. Reflectivity surface of DPCM-2IR as a function of coupling strengths Γ, Γ', for the ratio of input intensities $|q| = 1$, and for three different values of the transmissivity $|t|$, (a) $|t| = 0.9$, (b) $|t| = 0.2$, (c) $|t| = 0$. The reflectivity surface for the lossy DPCM is double valued, however the lower branch is unphysical.

q. One can write neat expressions for $|t| = 1$, [1] however this value is actually a singular point of the starting system of algebraic equations. Real solutions for u, u', a, a' do not exist there, and the threshold is pushed to $-\infty$. This is obvious if one considers the device with three IRs, as $t = 1$ means $u = -\pi/2$, and Eqs. (15a) and (15b) yield $a'' = 1$ and $\Gamma'' = -\infty$, which, of course, is not possible. Nonetheless, one can determine the thresholds and reflectivities numerically for all $|t| \neq 1$. From Figs. 5 and 6 it is obvious that they do not bear any resemblance to the 2Z-DPCM or the ICR. In fact, their behavior is quite the opposite.

This is corroborated by Fig. 7, which presents the cuts through the reflectivity surfaces of the 2Z-DPCM and the conserved DPCM with two IRs (DPCM-2IR). The figure depicts clearly the basic difference between these surfaces. The surface of 2Z-DPCM is locally hyperboloidal, and the surface of DPCM-2IR is ellipsoidal. The difference between the devices is essentially caused by making the input/output connection through the different (complementary) ports of the primed 4WM region, A'_{3d} in Fig. 1(a) and A'_{2d} in Fig. 2(c). Fig. 7 helps understand how do the two devices start to oscillate, and how do they reach the operation point. To this end, it helps to determine first the absolute threshold points on the threshold curves, i.e. the points where the total coupling strengths (equal to $\Gamma + \Gamma'$ for DPCM-2IR, and $\Gamma - \Gamma'$ for 2Z-DPCM) reach absolute minima.

To make matters simple, we discuss the case $|q| = 1$. The absolute threshold is found at the point where the line $\Gamma + \Gamma' = \text{const.}$ for DPCM-2IR, or the line $\Gamma - \Gamma' = \text{const.}$ for 2Z-DPCM, touches the threshold curve. It is also the point where the diagonal $\Gamma = \Gamma'$ (DPCM-2IR) or $\Gamma = -\Gamma'$ (2Z-DPCM) intersects the threshold curve. For DPCM-2IR this point has a straightforward meaning—it is the true absolute threshold, i.e. the smallest possible value of $|\Gamma + \Gamma'|$ for which

[1] In Ref. [4] a universal relation, as well as the defining equations for the conserved DPCM are written down explicitly for $|t| = |q| = 1$. These equations have no real solutions, and exhibit no threshold behavior, because $|t| = 1$ is the singular point. Nevertheless, what is claimed there is appropriate for the case $|t| \sim 0.5$.

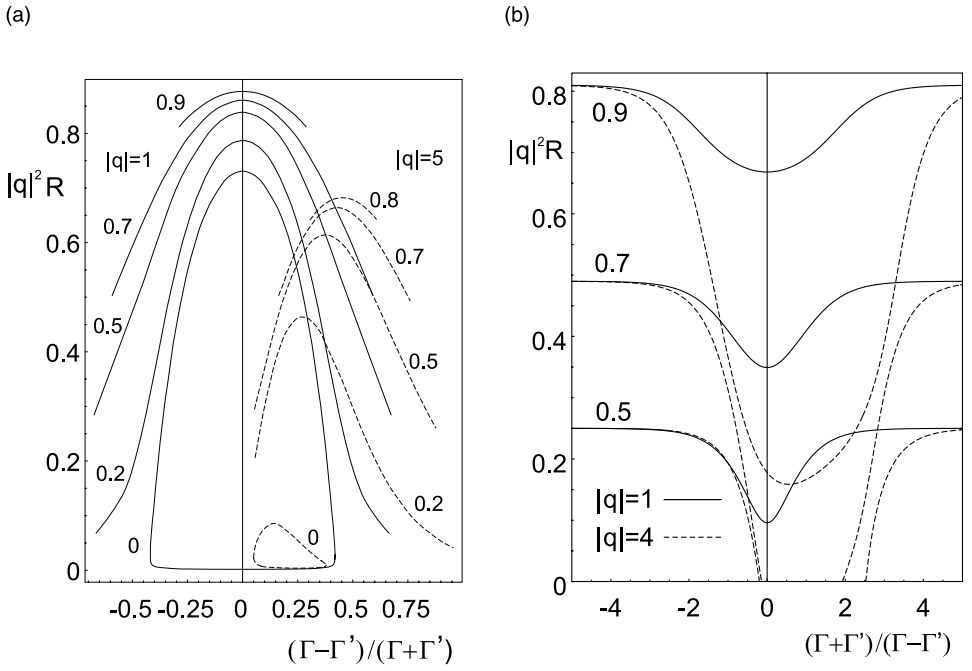

Fig. 7. (a) Cuts through the reflectivity surface of DPCM-2IR, for two values of $|q|$ and five values of $|t|$, given in the figure. The two curves for $|t| = 0$ form closed contours. The variable on the abscissa is a combination $(\Gamma - \Gamma')/(\Gamma + \Gamma')$ of coupling strengths, however the total coupling strength $\Gamma + \Gamma'$ is kept fixed at -7. (b) Cuts through the reflectivity surface of 2Z-DPCM, for two values of $|q|$ and three values of $|t|$, given in the figure. The variable combination is now $(\Gamma + \Gamma')/(\Gamma - \Gamma')$, and the total coupling strength $\Gamma - \Gamma'$ is fixed at -3.5.

the device will still work. It depends on $|t|$, and, for example, at $|t| = 0$ it is $\Gamma_{\text{th}} = \Gamma'_{\text{th}} = -2.49$, at $|t| = 0.5$ it is $\Gamma_{\text{th}} = \Gamma'_{\text{th}} = -1.79$, and at $|t| = 0.9$ it is $\Gamma_{\text{th}} = \Gamma'_{\text{th}} = -3.06$. For a fixed total coupling strength smaller than $|\Gamma_{\text{th}} + \Gamma'_{\text{th}}|$, the device does not function. For the total coupling strength larger than $|\Gamma_{\text{th}} + \Gamma'_{\text{th}}|$, there exists an interval $(\Delta\Gamma, \Delta\Gamma')$ about the absolute threshold point, in which the device can operate. These intervals are visible in Fig. 7(a), which is drawn for $\Gamma + \Gamma' = -7$. The point at which the device will operate is found where the reflectivity reaches the maximum. For $|q| = 1$ this happens at $\Gamma = \Gamma'$. Hence, the device prefers to operate at equal coupling strengths in the two IRs. For $|q| \neq 1$ the operation point shifts, and the device will operate at unequal coupling strengths. This is also visible in Fig. 7(a).

The situation with 2Z-DPCM is in a sense the opposite. For a fixed total coupling strength larger than $|\Gamma_{\text{th}} - \Gamma'_{\text{th}}|$, the device can function everywhere above the threshold (which is below the curve in Fig. 3(a)). At the absolute threshold point, the largest possible value of $|\Gamma - \Gamma'|$ is reached for which the device will not be working. At that point $\Gamma + \Gamma' = 0$. For a fixed total coupling strength smaller than $|\Gamma_{\text{th}} - \Gamma'_{\text{th}}|$, there exists an interval $(\Delta\Gamma, \Delta\Gamma')$ about the absolute threshold point, in which the device cannot operate. These intervals are visible in Fig. 7(b), which is drawn for $\Gamma - \Gamma' = -3.5$. For $|q| \neq 1$ the threshold point shifts. The operation point is still found where the reflectivity reaches maximum, however, there are now two disjoint operation intervals for a fixed total coupling strength $\Gamma - \Gamma'$. Hence, the device will try to move as much as possible away from the diagonal $\Gamma = -\Gamma'$, i.e. it will operate at the highest possible sum of the coupling strengths. This is reached at the border of the region of allowed coupling strengths.

5. Conclusions

We have analyzed the 2Z-DPCM device of Wolffer and Gravey [1] using the grating action method, and compared it with the supposedly equivalent devices, the ICR and the DPCM with double the interaction length. We find that ICR indeed is closely related to 2Z-DPCM, whereas the double DPCM is unrelated. In general, the various geometries of the two facing DPCMs are also unrelated to 2Z-DPCM, even though one can construct a geometry, the connected DPCM in this case, which is equivalent to ICR.

Apart from the connected DPCM, the closest DPCM-2IR comes to 2Z-DPCM is when the two IRs are adjacent to each other, forming the double DPCM, and the grating actions in 2Z-DPCM are of the same magnitude, but of the opposite sign. Then the equations for the grating actions in both devices have a similar form, however the equations for σ are still different. Hence, the thresholds and the operation behavior of the two devices will be different.

We have further established the threshold curves and the operation points of all these phase conjugation devices, and determined the reflectivities and the transmissivities as functions of both the grating actions and the coupling strengths.

An obvious but important point of difference between the 2Z-DPCM and ICR is that the redirection of interacting beams is achieved by mirrors in ICR, and by a lens in 2Z-DPCM. Clearly, the lens accomplishes more than simply redirecting and focusing the beams, it provides for aberrations necessary to eliminate conical diffraction. We do not address beam aberrations, nor the influence of the finite lateral extension of beams, which are important for the operation of 2Z-DPCM [1]. These questions lie outside the scope of the grating action method, which is based on the plane-wave approximation to the mixing of waves.

Finally, we note that the ICRs come in three different flavors, according to the types of diffraction gratings generated in the two interaction regions. There are the TG–TG rings, the RG–RG rings, and the mixed TG–RG rings [11,14]. Having in mind close relation between the TG–TG ring and 2Z-DPCM established here, it would be interesting to investigate experimentally whether it is possible to realize the RG–RG and the TG–RG 2Z-DPCM.

References

[1] N. Wolffer, P. Gravey, Opt. Commun. 107 (1994) 115.
[2] A.A. Zozulya, A.V. Mamaev, Sov. Phys. JETP 70 (1990) 56.
[3] M. Cronin-Golomb, B. Fischer, J.O. White, A. Yariv, IEEE J. Quant. Electron. QE-20 (1984) 12.
[4] M. Belić, M. Petrović, Z. Ljuboje, F. Kaiser, Opt. Commun. 143 (1997) 67.
[5] M. Belić, M. Petrović, O. Sandfuchs, F. Kaiser, Opt. Lett. 23 (1998) 340.
[6] M. Cronin-Golomb, Opt. Lett. 15 (1990) 897.
[7] M. Belić, M. Petrović, J. Opt. Soc. Am. B 11 (1994) 481.
[8] P. Yeh, Introduction to Photorefractive Nonlinear Optics, Wiley, New York, 1993.
[9] B. Fischer, S. Sternklar, S. Weiss, IEEE J. Quant. Electron. QE-25 (1989) 550.
[10] Z. Ljuboje, M. Belić, D. Vujić, F. Kaiser, J. Opt. Soc. Am. B 17 (2000) 1850;
M.R. Belić, How do photorefractive oscillators work, in: O.P. Nijhavan, A.K. Gupta, A.K. Musla, K. Singh (Eds.), Optics and Optoelectronics; Theory, Devices and Applications, vol. 2, Narosa Publishing Company, New Delhi, 1999, pp. 897–903.
[11] M. Belić, D. Vujić, J. Opt. A: Pure Appl. Opt. 2 (2000) 465.
[12] V.V. Eliseev, A.A. Zozulya, G.D. Bacher, J. Feinberg, J. Opt. Soc. Am. B 9 (1992) 398.
[13] S.G. Odulov, M.Y. Goulkov, O.A. Shinkarenko, Phys. Rev. Lett. 83 (1999) 3637.
[14] A.V. Mamaev, A.A. Zozulya, J. Opt. Soc. Am. B 8 (1991) 1447.